

2. Rogers JV, Mack LA, Freeny PC, et al. Hepatic focal nodular hyperplasia: angiography, CT, sonography, and scintigraphy. *Am J Roentgenol* 1981;137:983-990.
3. Yoshikawa J, Matsui O, Kadoya M, et al. Delayed enhancement of fibrotic areas in hepatic masses: CT-pathologic correlation. *J Comp Assist Tomogr* 1992;16:206-211.
4. Lee MJ, Saini S, Hamm B, et al. Focal nodular hyperplasia of the liver: MR findings in 35 proved cases. *Am J Roentgenol* 1991;156:317-320.
5. Shirkhoda A, Farah MC, Bernacki, et al. Hepatic focal nodular hyperplasia: CT and sonographic spectrum. *Abdom Imaging* 1994;19:34-38.
6. Kudo M, Tomita S, Tochio H, et al. Hepatic focal nodular hyperplasia: specific findings at dynamic contrast-enhanced US with carbon dioxide microbubbles. *Radiology* 1991;179:377-382.
7. Mathieu D, Bruneton JN, Drouillard J, et al. Hepatic adenoma and focal nodular hyperplasia: dynamic CT study. *Radiology* 1986;160:53-58.
8. Mattison GR, Glazer GM, Quint LE, et al. MR imaging of hepatic focal nodular hyperplasia: characterization and distinction from primary hepatic tumors. *Am J Roentgenol* 1987;148:711-715.
9. Butch RJ, Stark DD, Malt RA. MR imaging of hepatic focal nodular hyperplasia. *J Comp Assist Tomogr* 1986;10:874-877.
10. Nagorney DM. Benign hepatic tumors: focal nodular hyperplasia and hepatocellular adenoma. *World J Surg* 1995;19:13-18.
11. Cherqui D, Rahmouni A, Charlotte F, et al. Management of focal nodular hyperplasia and hepatocellular adenoma in young women: a series of 41 patients with clinical, radiological, and pathological correlations. *Hepatology* 1995;22:1674-1681.
12. Sandler MA, Petrocelli RD, Marks DS, et al. Ultrasonic features and radionuclide correlation in liver cell adenoma and focal nodular hyperplasia. *Radiology* 1980;135:393-397.
13. Biersack HJ, Thelen M, Torres JF, et al. Focal nodular hyperplasia of the liver as established by ^{99m}Tc-sulfur colloid and HIDA scintigraphy. *Radiology* 1980;137:187-190.
14. Shortell CK, Schwartz SI. Hepatic adenoma and focal nodular hyperplasia. *Surg Gynecol Obstet* 1991;173:426-431.
15. Calvet X, Pons F, Bruix J, et al. Technetium-99m-DISIDA hepatobiliary agent in diagnosis of hepatocellular carcinoma: relationship between detectability and tumor differentiation. *J Nucl Med* 1988;29:1916-1920.
16. Kurtaran A, Li SR, Raderer M, et al. Technetium-99m-galactosyl-neoglycoalbumin combined with iodine-123-(A14)-insulin visualizes human hepatocellular carcinomas. *J Nucl Med* 1995;36:1875-1881.
17. Virgolini I, Müller C, Klepetko W, et al. Decreased hepatic function in patients with hepatoma or liver metastasis monitored by hepatocytes specific galactosylated radioligand. *Br J Cancer* 1990;61:937-941.
18. Kudo M, Vera DV, Stadalnik RC. Hepatic receptor imaging using radiolabeled asialoglycoprotein analogs. In: Lee YC, Lee RT, eds. *Neoglycoconjugates: preparation and applications*. Orlando: Academic Press 1994;11:373-402.
19. Hickman J, Ashwell G. Studies on the hepatic binding of asialoglycoproteins by hepatoma tissue and by isolated hepatocytes. In: Tager JM, Hooghwinkel GJM, Daems WT, eds. *Enzyme therapy in lysosomal storage disease*. North-Holland, Amsterdam; 1974:169-172.
20. Stockert RJ, Becker FF. Diminished hepatic binding protein for desialy glycoproteins during chemical hepatocarcinogenesis. *Cancer Res* 1980;40:3632-3634.
21. Sawamura T, Nakada H, Hazama H, et al. Hyperasialoglyco-proteinemia in patients with chronic liver diseases and/or liver cell carcinomas. Asialoglycoprotein receptor in cirrhosis and liver cell carcinoma. *Gastroenterology* 1984;87:1217-1221.
22. Reimer P, Weissleder R, Lee AS, et al. Receptor imaging: application to MR imaging of the liver cancer. *Radiology* 1990;177:729-734.
23. Virgolini I, Kornek G, Höbart J, et al. Scintigraphic evaluation of functional hepatic mass in patients with advanced breast cancer. *Br J Cancer* 1993;68:549-554.
24. Virgolini I, Muller C, Hobart J, et al. Liver function in acute viral hepatitis as determined by a hepatocyte-specific ligand: ^{99m}Tc-galactosyl-neoglycoalbumin. *Hepatology* 1992;15:593-598.

Technetium-99m-Furifosmin as an Agent for Functional Imaging of Multidrug Resistance in Tumors

James R. Ballinger, Tassawwar Muzzammil and Malcolm J. Moore

Faculties of Pharmacy and Medicine, University of Toronto; Departments of Oncologic Imaging and Medical Oncology, Princess Margaret Hospital; and Division of Experimental Therapeutics, Ontario Cancer Institute, Toronto, Ontario, Canada

There has been a preliminary report that furifosmin, like the other lipophilic ^{99m}Tc cations sestamibi and tetrofosmin, is a substrate for P-glycoprotein, the membrane transporter that is a mechanism of multidrug resistance (MDR) in tumors. This has been further investigated in the rat mammary carcinoma cell line MatB/WT and its doxorubicin-selected resistant variant MatB/AdrR. **Methods:** In vitro studies were performed by adding furifosmin to stirred single-cell suspensions of MatB/WT and MatB/AdrR in the presence or absence of the Pgp-modulating drug PSC833. Dynamic imaging studies over 30 min were performed in rats bearing MatB/WT or MatB/AdrR tumors growing in the leg. **Results:** Accumulation of furifosmin in MatB/AdrR cells in vitro was much lower than that in MatB/WT cells. The addition of 1 μM PSC833 increased the plateau accumulation in MatB/AdrR cells 2.4-fold, but did not affect accumulation in MatB/WT cells. In rats, furifosmin accumulated rapidly in MatB/WT tumors and washed out with a mean t₃ of 78 min. Washout from MatB/AdrR tumors was more rapid, with a t₃ of 46 min (p < 0.025). Following dissection of animals at 30 min, mean tumor-to-muscle ratios were 1.57 and 1.05 in MatB/WT and MatB/AdrR tumors, respectively (p < 0.025). **Conclusion:** Furifosmin is suitable for functional imaging of multidrug resistance in tumors.

Key Words: technetium-99m-furifosmin; multidrug resistance; P-glycoprotein; breast cancer

J Nucl Med 1997; 38:1915-1919

Though developed as agents for myocardial perfusion imaging, both sestamibi and tetrofosmin have been useful for tumor imaging (1-6). In particular, sestamibi has been evaluated extensively for scintimammography and may play a role when the mammogram is indeterminate and in women who have dense breasts or who have had previous breast surgery (7-9). In screening the accumulation of sestamibi in a variety of tumor cell lines in vitro, Piwnicka-Worms' group noted that certain cell lines accumulated very little sestamibi (10). They later correlated this low accumulation with overexpression of P-glycoprotein (Pgp), a transmembrane pump that is a mechanism of multidrug resistance (MDR) in tumors (11). This work has been extended to insect cells transfected with the human *MDR1* gene (12) and to an animal model (13). Del Vecchio's group from Naples has presented results which show a correlation between sestamibi efflux rates and Pgp expression in biopsy samples (14,15) and response to chemotherapy (16) in patients with breast cancer. Other authors have also suggested that low accumulation of sestamibi corresponds to MDR in patients with lymphoma (17) and lung cancer (18).

We have demonstrated that tetrofosmin, a myocardial perfusion agent that is a phosphine rather than an isonitrile, is also a substrate for Pgp in vitro and has properties very similar to sestamibi (19).

Furifosmin is another ^{99m}Tc-labeled myocardial perfusion agent (20) that has been shown to be a substrate for Pgp in vitro (21). We have further evaluated this phenomenon, extending studies to an in vivo model of breast cancer, the results of which

Received Dec. 12, 1996; revision accepted Feb. 28, 1997.
For correspondence or reprints contact: J.R. Ballinger, PhD, Ontario Cancer Institute, 610 University Ave., Toronto, Ontario, Canada, M5G 2M9.

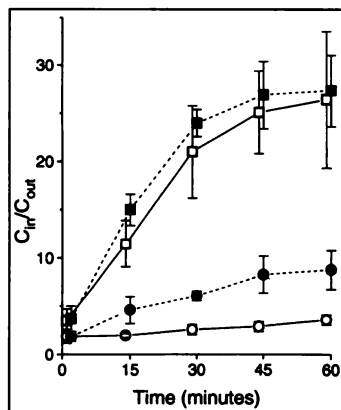


FIGURE 1. Time course of accumulation of ^{99m}Tc -furifosmin in MatB/WT and MatB/AdrR cells in the presence or absence of $1\ \mu\text{M}$ PSC833. Each point is the mean \pm s.d. of 3–5 separate experiments. □, MatB/WT; ■, MatB/WT + PSC833; ○, MatB/AdrR; ●, MatB/AdrR + PSC833.

suggest that furifosmin imaging can differentiate sensitive and MDR tumors.

MATERIALS AND METHODS

Reagents

Technetium-99m-furifosmin was prepared by reconstituting kits with $\sim 200\ \text{MBq}$ [^{99m}Tc]pertechnetate in 2 ml saline and heating in a boiling water bath for 10–15 min to complete the labeling reaction. Labeling efficiency, which was determined by thin-layer chromatography, was $>90\%$. This stock solution was then diluted to a working concentration of 10 MBq/ml with saline.

Modulator stock solutions were prepared fresh by dilution of pharmaceutical forms (cyclosporin A, verapamil) or ethanolic solution (PSC833) immediately before the experiments.

Cell Culture

The rat breast adenocarcinoma cell line MatB 13762 wild-type (MatB/WT) and its multidrug-resistant variant MatB/AdrR (22) were obtained from Dr. Gerald Batist, McGill University, Montreal, Canada. The MatB/AdrR cell line had been selected with doxorubicin and was confirmed in our laboratory to possess >200 -fold resistance to doxorubicin compared to the parental line. Cells were grown as monolayers in Nunclon tissue culture flasks in alpha-MEM medium supplemented with 10% fetal bovine serum. For in vitro experiments, cells were trypsinized, centrifuged and prepared as a single-cell suspension in fresh medium at a concentration of 1×10^6 cells/ml. For animal experiments, the same method was followed except that cells were resuspended at 1.2×10^6 cells/ml in phosphate-buffered saline.

In Vitro Studies

Cell suspensions were incubated with stirring in a water bath at 37°C under room air. At 1, 15, 30, 45 and 60 min after addition of ^{99m}Tc -furifosmin ($0.1\ \text{MBq/ml}$ final concentration) to the cell suspensions, duplicate samples of $500\ \mu\text{l}$ were taken and transferred to 1.5-ml microcentrifuge tubes containing $500\ \mu\text{l}$ ice-cold saline. After the tubes had been centrifuged at 12,000 rpm for 2 min, $100\text{-}\mu\text{l}$ aliquots of supernatant were transferred to counting tubes. The remaining supernatant was aspirated and the pellets were washed gently with 1 ml ice-cold saline. The tips of the tubes containing the pellets were then clipped into counting tubes and the radioactivity was measured at 90–190 keV in a gamma well counter. The accumulation ratio was calculated as the ratio of radioactivity concentration inside the cell to that in an equal volume of supernatant medium as described previously (13,19). For experiments in which modulator effects were assessed, the modulator (verapamil, cyclosporin A, or PSC833, a potent, non-immunosuppressive, non-nephrotoxic analog of cyclosporin) was added at the desired concentration 5–10 min before the tracer.

Parallel studies were performed with flow cytometry using fluorescence of daunorubicin at a concentration of $2\ \mu\text{g/ml}$ in the

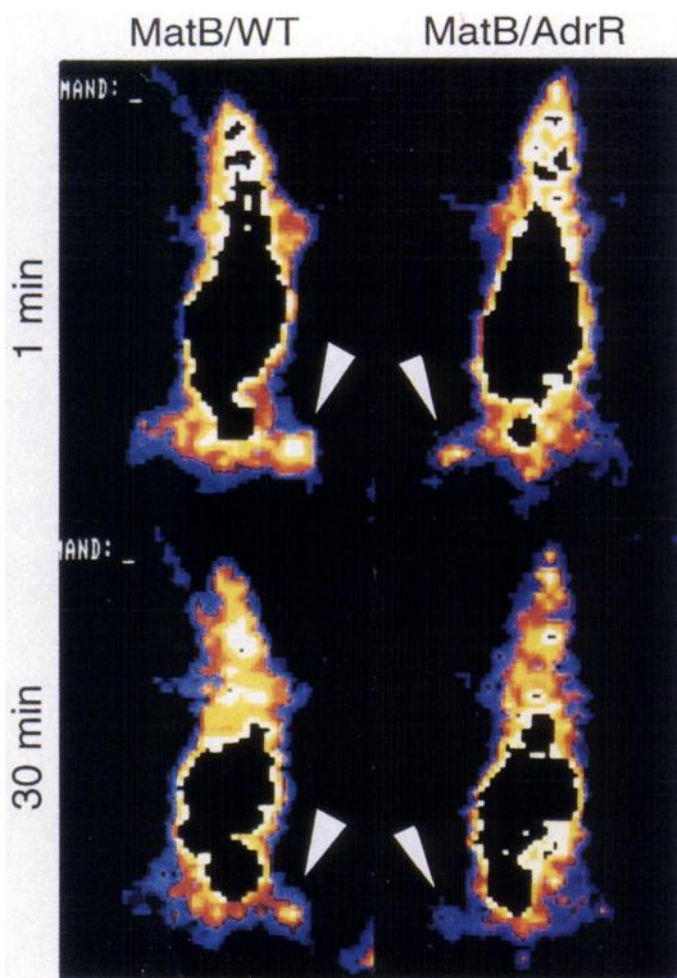


FIGURE 2. Gamma camera images of rats bearing MatB/WT (left column) or MatB/AdrR tumors (right column) implanted in the leg (arrow). Images were acquired for 60 sec at 1 min (upper row) or 30 min (lower row) after injection of 2 MBq furifosmin via a cannula in the jugular vein.

absence or presence of $2\ \mu\text{M}$ cyclosporin A. The instrument (EPICS, Coulter Electronics, Hialeah, FL) had an excitation at 488 nm and emission at 575 nm.

Animal Studies

Female Fisher 344 rats, 8–10 wk old, received a bolus injection of 5×10^5 cells in $400\ \mu\text{l}$ subcutaneously in the upper hind leg. When the tumors reached a diameter of 5–10 mm, the animals were prepared for imaging. The animals were anesthetized with intraperitoneal ketamine/xylazine (1:2), and the jugular vein was dissected and cannulated as a route for drug administration. Imaging was performed on a gamma camera equipped with a low-energy, all-purpose, parallel-hole collimator and interfaced to a computer. Anesthetized animals were placed prone on the face of the collimator with their legs fully extended to allow visualization of the tumor. Technetium-99m-furifosmin ($2\ \text{MBq}$ in $0.2\ \text{ml}$) was administered as a bolus via the jugular cannula followed by a saline flush to clear the line. Dynamic images were obtained at 1 frame/min beginning immediately upon injection and continuing for 30 min. The images were later analyzed for tracer efflux rates by defining and marking the region of interest (ROI) as the area of the tumor showing highest activity and recording tracer counts over this area for each of the 30 frames. These counts were normalized to the peak counts and fitted to a monoexponential equation by the method of least squares to allow calculation of tracer efflux rate as described previously (13). The animals were euthanized by barbiturate overdose at the end of the imaging session and samples of

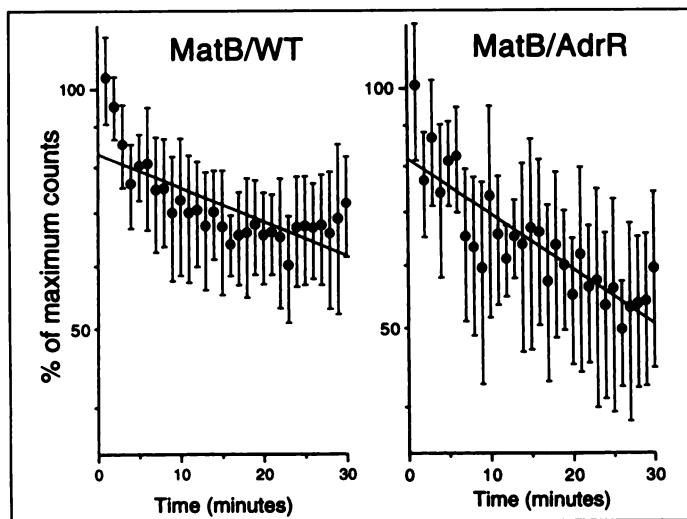


FIGURE 3. Time-activity curves for furifosmin in MatB/WT or MatB/AdrR tumors in rats. Each point is mean \pm s.d. for 10 animals. Efflux half-times were calculated by fitting data to a monoexponential equation.

blood, kidney, liver, heart, tumor and skeletal muscle were taken in that order. These samples were weighed and assayed for tracer radioactivity, and the percent injected dose per gram of tissue was calculated. Statistical comparisons were made using Student's t-test for unpaired data.

RESULTS

In Vitro Studies

Furifosmin partitioned rapidly into MatB/WT cells and accumulated in a linear fashion for 30 min, after which the rate of accumulation slowed and the ratio of radioactivity concentration inside the cell to that outside (C_{in}/C_{out}) reached a plateau value of 26.4 ± 7.1 (mean \pm s.d.) by 60 min (Fig. 1). In contrast, accumulation of furifosmin in MatB/AdrR cells was much slower and reached a value of only 3.6 ± 0.5 by 60 min, for a MatB/WT-to-MatB/AdrR differential of 7-fold. The addition of $1 \mu\text{M}$ PSC833, a modulator of Pgp function, to the medium did not significantly affect the accumulation of furifosmin in MatB/WT cells, but the same concentration of PSC833 produced a 2.4-fold increase in the accumulation of furifosmin in MatB/AdrR cells over 60 min. From experiments carried out with the addition of different concentrations of modulators, the rank order of potency of modulators was PSC833 > cyclosporin A > verapamil, with each difference being approximately one order of magnitude (data not shown).

By using flow cytometry, daunorubicin fluorescence in MatB/WT cells was 15.0 mean fluorescence units, which increased only slightly to 16.3 units when $2 \mu\text{M}$ cyclosporin A were added. In contrast, daunorubicin fluorescence was 2.4 units in MatB/AdrR cells, which increased to 15.9 units upon addition of cyclosporin A. Thus, the MatB/WT-to-MatB/AdrR differential of sixfold in daunorubicin content is similar to the sevenfold differential in furifosmin content previously mentioned.

Animal Studies

When administered to tumor-bearing rats as a bolus via an intravenous cannula, furifosmin distributed rapidly throughout the body, with the greatest amounts of radioactivity accumulating in the liver and kidneys. Excretion into the urinary bladder was evident by 3 min after injection and the bladder quickly became the organ with the highest amount of radioactivity. Clearance through the liver was also seen over 30 min.

TABLE 1
Tissue Distribution of Furifosmin 30 Min after Intravenous Administration to Rats Bearing MatB/WT or MatB/AdrR Tumors

Parameter	MatB/WT	MatB/AdrR	t-test
% Injected dose per gram tissue			
Blood	0.18 ± 0.11	0.18 ± 0.13	ns
Heart	1.51 ± 0.64	1.49 ± 0.48	ns
Liver	0.44 ± 0.26	0.38 ± 0.15	ns
Kidneys	3.35 ± 1.27	3.16 ± 0.80	ns
Muscle	0.17 ± 0.07	0.13 ± 0.05	ns
Tumor	0.25 ± 0.08	0.13 ± 0.07	$p < 0.005$
Tumor-to-Blood Ratio	1.67 ± 0.53	0.82 ± 0.36	$p < 0.001$
Tumor-to-Muscle Ratio	1.57 ± 0.41	1.05 ± 0.42	$p < 0.0025$

Each value is mean \pm s.d. for 10 rats.

As shown in Figure 2, the upper threshold had been reduced to mask radioactivity in the liver, kidneys and bladder and allow tumor visualization. The same threshold was used for MatB/WT and MatB/AdrR images at each time point. In the images obtained at 1 min postinjection (upper row), both the MatB/WT and MatB/AdrR tumors are clearly seen. In contrast, in the 30-min postinjection images (lower row), the MatB/WT tumor is still visible, but most of the radioactivity had washed out of the MatB/AdrR tumor.

Quantification was performed by drawing an ROI around the tumor on the 1-min image and recording the counts in that ROI in each of the 30 images. The tumor activity in the images obtained at 1 min reflects perfusion and did not differ between MatB/WT and MatB/AdrR tumors when corrected for tumor weight. Washout rates were calculated from the time-activity curves and yielded half-times of 78 ± 36 min for MatB/WT tumors and 46 ± 17 min for MatB/AdrR tumors ($p < 0.025$). The mean data and fitted monoexponential equations are presented in Figure 3.

Following the 30-min imaging study, the rats were euthanized and dissected, and the tissues were assayed in a gamma counter. Biodistribution data are summarized in Table 1 and indicate that radioactivity in normal tissues did not differ between rats bearing MatB/WT or MatB/AdrR tumors. In contrast, radioactivity in the MatB/AdrR tumors, despite similar perfusion as documented above, was significantly lower than that in MatB/WT tumors whether expressed as the percent injected dose per gram, tumor-to-blood ratio or tumor-to-muscle ratio.

TABLE 2
Comparison of Properties of Furifosmin, Sestamibi and Tetrofosmin in MatB/WT and MatB/AdrR Cells In Vitro

Parameter	Furifosmin (this work)	Sestamibi (13)	Tetrofosmin (19)
C_{in}/C_{out} ratio @ 60 min			
MatB/WT	26.4 ± 7.1	218 ± 19	70.9 ± 15.0
MatB/AdrR	3.6 ± 0.5	13.3 ± 2.0	2.8 ± 1.0
WT/AdrR ratio	7.3	16.4	25.3
Enhancement by $1 \mu\text{M}$ PSC833 @ 60 min			
(MatB/AdrR + PSC833) / (MatB/AdrR - PSC833)	2.4	8.9	11

Each value is mean or mean \pm s.d. for 3-5 experiments.

TABLE 3

Comparison of Properties of Furifosmin, Sestamibi, and Tetrofosmin in Rats Bearing MatB/WT or MatB/AdrR Tumors

Parameter	Furifosmin	Sestamibi	Tetrofosmin
Efflux $t_{1/2}$ (min)			
MatB/WT	78 ± 36 (10)	119 ± 29 (5)	81 ± 36 (4)
MatB/AdrR	46 ± 17 (10)	47 ± 17 (4)	n.d.
Tumor-to-Muscle ratio @ 30 min.			
MatB/WT	1.57 ± 0.41 (10)	1.69 ± 0.45 (7)	1.88 ± 0.32 (4)
MatB/AdrR	1.05 ± 0.42 (10)	1.13 ± 0.09 (4)	n.d.

Each value is mean ± s.d. for (n) rats

DISCUSSION

It has recently been reported that furifosmin is a transport substrate for Pgp (21). In the present work, the accumulation characteristics of furifosmin in a rat breast cancer cell line, MatB/WT, and its doxorubicin-selected resistant variant, MatB/AdrR, are compared to those of sestamibi (13) and tetrofosmin (19) in vitro and in vivo. Qualitatively, the in vitro behavior of the three tracers is similar in that MatB/WT cells accumulate much more radioactivity than MatB/AdrR cells, and the addition of a Pgp modulator such as PSC833 increases the accumulation in MatB/AdrR cells but not in MatB/WT cells. However, there are quantitative differences as seen in Table 2. The rank order of absolute accumulation (i.e., plateau C_{in}/C_{out} value) in MatB/WT cells is sestamibi > tetrofosmin > furifosmin, whereas for the difference between MatB/WT and MatB/AdrR cells, the sequence is tetrofosmin > sestamibi > furifosmin. Sestamibi and tetrofosmin are similar in their response to modulating agents (enhancement by 1 μ M PSC833 and EC_{50} values), while the amplitude of furifosmin enhancement is not as great but occurs at similar EC_{50} values.

Both MatB/WT and MatB/AdrR tumors could be visualized immediately following intravenous administration of furifosmin to rats. However, over the course of 30 min, the radioactivity washed out of the MatB/AdrR tumors more rapidly than it did from MatB/WT tumors, and at the end of that time the MatB/AdrR tumors were barely visible (Fig. 2). As with sestamibi (13), image manipulation by thresholding was required to allow visualization of the tumor because of radioactivity retention in the abdomen; however, in the comparison images presented in Figure 2, the degree of thresholding was identical for MatB/WT and MatB/AdrR tumors at each time point. The washout rate of furifosmin from the tumor was fit to a monoexponential function with half-times of 78 and 46 min for the MatB/WT and MatB/AdrR tumors, respectively (Fig. 3). It is evident that a monoexponential function does not adequately describe the efflux pattern, but this approach was used for comparative purposes.

These results can be compared with data for sestamibi obtained previously in the same animal model at our institution (13). As seen in Table 3, sestamibi washout half-times were comparable to those obtained with furifosmin except that the washout of sestamibi from MatB/WT tumors was slower than that of furifosmin. The tumor-to-muscle ratios obtained from the dissected tissues were very similar for furifosmin and sestamibi (Table 3). In a limited number of in vivo experiments with tetrofosmin in MatB/WT tumors, the efflux rate and

tumor-to-muscle ratio at 30 min were also similar to the values obtained with the other two tracers (Table 3).

Furifosmin (Q12) is a member of a class of mixed-ligand ^{99m}Tc cations known as Q-complexes. Several of these analogs have been shown to be transport substrates for Pgp in vitro (21,23). Two in particular, Q58 and Q63, demonstrate in vitro properties that are far superior to those seen with furifosmin in terms of differential between levels of accumulation in WT and resistant cells and in response to Pgp modulation (23). The results in the present article, which show that furifosmin can image MDR, make it important to evaluate these new analogs whose in vitro properties suggest they might offer improved signal-to-noise ratios and tissue contrast.

ACKNOWLEDGMENTS

We thank Dr. Gerald Batist, McGill University, for supplying the MatB cell lines, Dr. David Hedley for assistance with flow cytometry, and Patricia Firby and Meili Li for assistance in setting up the model systems. Cyclosporin A (Sandimmune) and PSC833 were donated by Sandoz Canada. Financial support was provided by a grant from Mallinckrodt Medical Inc., St. Louis, MO.

REFERENCES

- Piwnic-Worms D, Holman BL. Noncardiac applications of hexakis(alkylisonitrile) technetium-99m complexes. *J Nucl Med* 1990;31:1166-1167.
- Caner B, Kitapci M, Aras T, Erbeni G, Ugur O, Bekdik C. Increased accumulation of hexakis (2-methoxyisobutylisonitrile)technetium(I) in osteosarcoma and its metastatic lymph nodes. *J Nucl Med* 1991;32:1977-1978.
- Baillet G, Albuquerque L, Chen Q, Poisson M, Delattre J-Y. Evaluation of single-photon emission tomography imaging of supratentorial brain gliomas with technetium-99m-sestamibi. *Eur J Nucl Med* 1994;21:1061-1066.
- Mansi L, Rambaldi PF, La Provitiera A, Di Gregorio F, Procaccini E. Technetium-99m-tetrofosmin uptake in breast tumors [Abstract]. *J Nucl Med* 1995;36(suppl):83P.
- Basoglu T, Sahin M, Coskun C, Koparan A, Bernay I, Erkan L. Technetium-99m-tetrofosmin uptake in malignant lung tumors. *Eur J Nucl Med* 1995;22:687-689.
- Klain M, Maurea S, Lastoria S, Cuocolo A, Colao A, Salvatore M. Technetium-99m-tetrofosmin imaging of differentiated mixed thyroid cancer. *J Nucl Med* 1995;36:2248-2251.
- Khalkhali I, Mena I, Diggles L. Review of imaging techniques for the diagnosis of breast cancer: a new role of prone scintimammography using technetium-99m-sestamibi. *Eur J Nucl Med* 1994;21:357-362.
- Taillefer R, Robidoux A, Lambert R, Turpin S, Laperriere J. Technetium-99m-sestamibi prone scintimammography to detect primary breast cancer and axillary lymph node involvement. *J Nucl Med* 1995;36:1758-1765.
- Khalkhali I, Cutrone J, Mena I, et al. Technetium-99m-sestamibi scintimammography of breast lesions: clinical and pathological follow-up. *J Nucl Med* 1995;36:1784-1789.
- Delmon-Moingeon LI, Piwnica-Worms D, Van den Abbeele AD, Holman BL, Davison A, Jones AJ. Uptake of the cation hexakis(2-methoxyisobutylisonitrile)-technetium-99m by human carcinoma cell lines in vitro. *Cancer Res* 1990;50:2198-2202.
- Piwnic-Worms D, Chiu ML, Budding M, Kronauge JF, Kramer RA, Croop JM. Functional imaging of multidrug-resistant P-glycoprotein with an organotechnetium complex. *Cancer Res* 1993;53:977-984.
- Rao VV, Chiu ML, Kronauge JF, Piwnica-Worms D. Expression of recombinant human multidrug resistance P-glycoprotein in insect cells confers decreased accumulation of technetium-99m-sestamibi. *J Nucl Med* 1994;35:510-515.
- Ballinger JR, Hua HA, Berry BW, Firby P, Boxen I. Technetium-99m-sestamibi as an agent for imaging P-glycoprotein-mediated multi-drug resistance: in vitro and in vivo studies in a rat breast tumour cell line and its doxorubicin-resistant variant. *Nucl Med Commun* 1995;16:253-257.
- Del Vecchio S, Ciarmiello A, Potena MI, et al. In vivo detection of multidrug-resistant (MDRI) phenotype by technetium-99m-sestamibi scan in untreated breast cancer patients. *Eur J Nucl Med* 1997;24:150-159.
- Del Vecchio S, Ciarmiello A, Pace L et al. Fractional retention of technetium-99m-sestamibi as an index of P-glycoprotein expression in untreated breast cancer. *J Nucl Med* 1997;38:1348-1351.
- Ciarmiello A, Del Vecchio S, Potena MI, et al. Technetium-99m-sestamibi efflux and therapeutic response in patients with advanced breast carcinoma [Abstract]. *Proc Am Assoc Cancer Res* 1996;37:310.
- Dimitrakopoulou-Strauss A, Strauss LG, Goldschmidt H, Lorenz WJ, Maier-Borst W, van Kaick G. Evaluation of tumor metabolism and multidrug resistance in patients with treated malignant lymphomas. *Eur J Nucl Med* 1995;22:434-442.
- Moretti JL, Caglar M, Boaziz C, Caillat-Vigneron N, Moree JF. Sequential functional imaging with technetium-99m-hexakis-2-methoxyisobutylisonitrile and indium-111-octreotide: can we predict the response to chemotherapy in small cell lung cancer? *Eur J Nucl Med* 1995;22:177-180.
- Ballinger JR, Bannerman J, Boxen I, Firby P, Hartman NG, Moore MJ. Technetium-99m-tetrofosmin as a substrate for P-glycoprotein: in vitro studies in multidrug-resistant breast tumor cells. *J Nucl Med* 1996;37:1578-1582.

20. Rossetti C, Vanoli G, Paganelli G, et al. Human biodistribution, dosimetry, and clinical use of technetium(III)-99m-Q12. *J Nucl Med* 1994;35:1571-1580.
21. Crankshaw CL, Marmion M, Burleigh BD, Deutch E, Piwnica-Worms D. Nonreducible mixed ligand Tc(III) cations (Q complexes) are recognized as transport substrates by the human multidrug resistance (MDR) P-glycoprotein [Abstract]. *J Nucl Med* 1995;36(suppl):130P.
22. Schechter RL, Woo A, Duong M, Batist G. In vitro and in vivo mechanisms of drug resistance in rat mammary carcinoma model. *Cancer Res* 1991;51:1434-1442.
23. Luker G, Crankshaw CL, Marmion M, Burleigh BD, Deutsch E, Piwnica-Worms D. Mixed ligand Tc-99m(III) cations (Q-complexes) are recognized as transport substrates by the human multidrug resistance P-glycoprotein [Abstract]. *Proc Am Assoc Cancer Res* 1996;37:317.

Radiation Dosimetry for Indium-111-Pentetreotide

M.G. Stabin, P.P.M. Kooij, W.H. Bakker, T. Inoue, K. Endo, J. Coveney, R. de Jong and A. Minegishi
Oak Ridge Institute for Science and Education, Oak Ridge, Tennessee; University Hospital Dijkzigt, Rotterdam, The Netherlands; Gunma University, Gunma, Japan; Mallinckrodt, Inc., St. Louis, Missouri; Mallinckrodt Medical, B.V., Petten, Holland; IBRD Japan Corporation, Tokyo, Japan

We present radiation dose estimates for ^{111}In -pentetreotide. **Methods:** Kinetic data were gathered in 10 subjects at two different sites. A compartmental model was used to fit the data, including retention, in three major organs and excretion. **Results:** The data were consistent for the subjects at both sites. The organ receiving the highest dose was the kidneys (0.52 mGy/MBq); the effective dose equivalent was 0.1 mSv/MBq, and the effective dose was 0.073 mSv/MBq. **Conclusion:** The results of this study provide the basis for evaluation of radiation safety of this drug.

Key Words: dosimetry; indium-111-pentetreotide; somatostatin receptors; brain

J Nucl Med 1997; 38:1919-1922

The molecule ^{123}I -tyrosine (Tyr) (3)-octreotide is a somatostatin receptor imaging agent for use in the scintigraphic localization of neuroendocrine tumors (1). A similar molecule, pentetreotide, has been successfully labeled with ^{111}In complexed to the diethylenetriamine pentaacetic acid (DTPA) molecule and shows improved clinical results when used to study this system (2), due to higher renal clearance relative to hepatobiliary clearance. This article presents the radiation dosimetry of ^{111}In -DTPA-labeled pentetreotide based on two separate human studies involving a total of 10 patients. All results from the two studies will be shown; we believe that the results are in agreement and that a combined result, using data from all 10 patients, is recommended to establish the radiation dosimetry of this agent. It is hoped that the data presented in this article will be useful to regulators, users and others in understanding the radiation dosimetry of this agent in adults. The extension of these results to children and pregnant women will be discussed briefly.

MATERIALS AND METHODS

Human studies were undertaken by the University Hospital Dijkzigt in Rotterdam, the Netherlands, and at Gunma University in Gunma, Japan. The study in Holland involved six subjects; the study in Japan involved four subjects. In each study, ^{111}In -DTPA pentetreotide was administered to the subjects in quantities typical of a clinical imaging study, and the subsequent retention and excretion was studied through a combination of quantitative gamma camera imaging and urine collection and analysis. Fecal analysis was performed in only four subjects; it was thought that this pathway would not be very significant. The modeling results

and a limited number of analyzed samples predicted a fairly low average gastrointestinal (GI) tract clearance (around 0.5%–2%, see Results), which agreed with the impressions from the gamma camera images. The methods for imaging and image quantitation are described in other works (3,4), although the energy windows in the Bakker et al. study (3) were changed from those used for ^{123}I to ensure their appropriateness for ^{111}In imaging. Briefly, in the studies conducted in the Netherlands, planar images were obtained with a large field of view camera equipped with a parallel-hole collimator. Anterior and posterior whole-body scintigrams were taken at 30 min postinjection, and again at 4 and 24 hr, and, in some cases, at 48 hr. Radioactivity in the blood, urine and feces was collected at various intervals over the course of the study, up to 48 hr, and measured in either a dose calibrator or a GeLi detector system. In the Japanese studies, anterior and posterior images were taken at 30 min and at 1, 2, 4, 6, 24 and 48 hr postinjection. Whole-body and SPECT imaging was performed using a gamma camera equipped with a medium-energy collimator. A 20% energy window centered at 173 and 247 keV was used. Geometric means of the anterior and posterior counts in regions of interest over the major organs were calculated. Urine samples were also collected at various times over the course of the study (to 48 hr) and analyzed in a dose calibrator.

Time-activity data gathered in the human studies were expressed as a percent of the administered activity and fit with a compartment model (Fig. 1) using the Simulation, Modeling and Analysis (SAAM) software (5). This model, when solved, is meant only to be descriptive of the observed kinetics of this agent for the purpose of developing radiation dose estimates. It generally provides two compartments to represent most organs and has two pathways for handling excretion (urinary and fecal). Areas under the time-activity curves for most organs were estimated directly from the fitted functions integrated over time and expressed as residence times (6). In the case of the urinary bladder, the program fit the cumulative urine activity curve, and then the bladder was assumed to void every 4.8 hr. The residence time for the bladder was then integrated from the time-activity curve assuming this voiding pattern. Activity entering the GI tract was assumed to clear through the gallbladder, small intestine, upper large intestine and lower large intestine according to the kinetics, as published previously (7).

Absorbed dose estimates were calculated using the standard MIRD technique (6), implemented in the MIRDOSE 3.1 computer software (8). The effective dose equivalent, as defined in ICRP Publication 30 (7), and the effective dose, as defined in ICRP Publication 60 (9), are shown in the tables. There is currently some

Received Feb. 15, 1996; revision accepted Feb. 21, 1997.

For correspondence or reprints contact: Michael G. Stabin, PhD, Oak Ridge Institute for Science and Education, P.O. Box 117, Oak Ridge, TN 37831-0117.